TU Delft

Delft University of Technology

3D concrete printing

Lattice modeling of structural failure considering damage and deformed geometry

Chang, Ze; Liang, Minfei; Xu, Yading; Schlangen, Erik; Šavija, Branko

DOI
10.1016/j.cemconcomp.2022.104719

Publication date
2022

Document Version
Final published version

Published in
Cement and Concrete Composites

Citation (APA)
Chang, Z., Liang, M., Xu, Y., Schlangen, E., & Šavija, B. (2022). 3D concrete printing: Lattice modeling of structural failure considering damage and deformed geometry. *Cement and Concrete Composites*, *133*, Article 104719. https://doi.org/10.1016/j.cemconcomp.2022.104719

Important note
To cite this publication, please use the final published version (if applicable).
Please check the document version above.

Copyright
Other than for strictly personal use, it is not permitted to download, forward or distribute the text or part of it, without the consent of the author(s) and/or copyright holder(s), unless the work is under an open content license such as Creative Commons.

Takedown policy
Please contact us and provide details if you believe this document breaches copyrights.
We will remove access to the work immediately and investigate your claim.

This work is downloaded from Delft University of Technology.
For technical reasons the number of authors shown on this cover page is limited to a maximum of 10.

Cement and Concrete Composites 133 (2022) 104719

Contents lists available at ScienceDirect

Cement and Concrete Composites

journal homepage: www.elsevier.com/locate/cemconcomp

3D concrete printing: Lattice modeling of structural failure considering damage and deformed geometry

Ze Chang, Minfei Liang *, Yading Xu, Erik Schlangen, Branko Šavija

Microlab, Faculty of Civil Engineering and Geosciences, Delft University of Technology, 2628 CN, Delft, the Netherlands

ARTICLE INFO

Keywords:
Incremental analysis
Load-unload method
Buildability quantification
Deformation history

ABSTRACT

This research studies the impact of localized damage and deformed printing geometry on the structural failure of plastic collapse for 3D concrete printing (3DCP) using the lattice model. Two different approaches are utilized for buildability quantification: the (previously developed) load-unload method, which updates and relaxes the printing system after each analysis step and repeatedly applies the gravitational loading to the undeformed structure; and the incremental method, which keeps the load after each analysis step and applies the incremental loading to the deformed printing system. The former can consider the material yielding but cannot capture accurately the structural deformation during printing process. Compared to the load-unload method, the incremental method can not only consider deformed printing geometry but can also simulate the non-proportional loading conditions and disequilibrium force occurring during 3D printing. In this study, computational uniaxial compression tests are first conducted to compare two algorithms. The numerical results indicate the consideration of nonequilibrium force and deformed geometry affects the peak load and crack information for fracture analysis. Subsequently, the incremental method is incorporated into the lattice model to quantify buildability of 3DCP. The predictions are compared with previously published numerical results obtained using the load-unload method. The lattice model based on incremental method reproduces correct failure mode; better quantitative agreement about critical printing height also can be obtained. These numerical analyses demonstrate that the incremental solution is an approximate method for buildability quantification since it can account for the nonequilibrium force induced by the deformed printing geometry and localized damage.

1. Introduction

Extrusion-based 3D concrete printing (3DCP) enables to build structural components from a digital model with limited or no need for temporary formwork. Initially proposed by Pegna [1], 3DCP has gained growing attention in the field of concrete construction over the past decades [2–5]. This layer-by-layer manufacturing process outperforms conventional methods in many aspects, such as reduction in cost and construction time and minimization of material usage [3,6]. Using this advanced technology, some large-scale structures have been successfully constructed [7,8], clearly showing a promising future of 3DCP in the construction industry.

For a successful printing procedure, on the one hand, layers of designed objects should be deposited smoothly from the printhead without segregation and blockage [9,10]; after material deposition, on the other hand, the printed segments must be strong enough to withstand their self-weight and carry additional loading from subsequent printing layers without excessive deformation or structural failure. Therefore, understanding the rheological and mechanical behaviors of printable materials plays a significant role in mix design to meet requirements of flowability, extrudability as well as buildability [11–13]. The flowability and extrudability are associated with rheological behaviors of printable materials, namely the yield stress and viscosity, and a recent article gives a good overview of this process [14].

For buildability, the stepwise load increments due to the self-weight of successive printing layers result in structural failure of elastic buckling or plastic collapse. Two competing age-dependent processes codetermine the structural buildability of a printing object. The material stiffness and strength increase due to hydration to support the increasing gravitational loading from more printing layers [15–17]. Currently, several experimental methods, such as the green strength test [15,18,19], direct shear test [11,15], triaxial compression test [20], and vane shear test [10,21], are being used for measuring material properties relevant to structural buildability. In addition, a series of analytical and

* Corresponding author.
E-mail address: m.liang-1@tudelft.nl (M. Liang).

https://doi.org/10.1016/j.cemconcomp.2022.104719
Received 9 March 2022; Received in revised form 19 June 2022; Accepted 8 August 2022
Available online 13 August 2022
0958-9465/© 2022 The Author(s). Published by Elsevier Ltd. This is an open access article under the CC BY license (http://creativecommons.org/licenses/by/4.0/).

Table 1
Different methodologies for buildability quantification in 3D concrete printing.

	Theoretical framework/ model type	Model description	Model application	Model limitation	Main contributors	Others
1	Rheology/ Analytical model	The model proposes several rheological requirements on printable materials considering flocculation-induced thixotropy and chemical reaction	Analytical models consider the development of materials properties and printing velocity to estimate structural failure due to plastic collapse while the printing process	Geometry limitation, structural variability	Roussel [13]	[11,12, 31–33]
		The model accounts for the re-flocculation and structuration thixotropy mechanisms			Kruger et al. [22,23,34]	
		The model proposes linear and non-linear curing function			Perrort et al. [24]	
2	Solid mechanics/ Analytical model	The mechanistic model includes a series of printing parameters for the prediction of elastic buckling and plastic collapse	The model studies impact of printing velocity, curing function, geometrical features, and material heterogeneity	Geometry limitation, structural variability	Suiker [26,27]	[19,33]
3	Fluid dynamics model /Numerical model	Computational fluid dynamics models use generalized Newtonian fluid and elastic-viscous-plastic fluid constitutive relationship	The relationship between the cross-sectional shape of printing segments and printing parameters, including printing speed, nozzle height, and extrusion force is established	Buckling failure, localized damage	R. Comminal et al. [28–30]	
4	Solid mechanics /Numerical model	FEM-based numerical models adopt time-dependent elastic-plastic behavior and Mohr-Coulomb criterion	Plastic collapse and elastic buckling	Localized damage, structural failure criterion	Wolfs et al. [15, 17,20]	[10,11, 14, 35–37]
		The extended lattice model considers time-dependent material properties and non-uniform gravitational loading	Plastic collapse failure mode	Deformation history, buckling failure	Chang et al. [38,39]	

numerical models have been proposed to assess when and how a printing object may fail. Such tools can replace or at least decrease the trial-and-error testing, which is resource- and time-consuming.

These analytical and numerical models can be classified into four categories on a basis of fundamental theory, as listed in Table 1. The first category comprises analytical models based on rheology theory, and the typical research work is from Roussel [13]. Other notable contributions encompass the lower bound analytical model from Kruger et al. [22,23], and the empirical linear and non-linear model from Perrot et al. [24,25]. These rheological models allow for the effect of flocculation-induced thixotropy and chemical reaction on material yield stress, thereby predicting critical printing height considering material yielding. The main advantage of these analytical methods is that they can be easily rewritten to define allowable printing speed in preventing structural failure based on the time-dependent material properties. Nevertheless, these analytical models do not consider the variations of process parameters or the gradient of material stiffness/strength over object height [3]. The second category is the mathematical model proposed by Suiker [26] based on solid mechanics. Through this model, the structural failure due to plastic collapse and elastic buckling can be predicted and the results show quantitative agreements with experimental data and other numerical results [17,27]. However, similar to other analytical models, it is also limited to the specific printing geometry; furthermore, geometric or material imperfections due to the printing process cannot be considered. In pursuit of more accurate quantification on structural buildability, the use of numerical models seems to be a preferred solution.

The third category comprises computational fluid dynamics models (CFD) [28,29]. Two formulations of the constitutive law are considered: the generalized Newtonian and elastic-viscous-plastic fluid. A recently published work extends the model application to layer deformation after material deposition [30]. Using this kind of model, the correlations between the cross-sectional shape of printing segments and printing parameters, including printing speed, nozzle height, and extrusion force, can be established. More research towards buildability quantification is expected by virtue of CFD.

The last category comprises numerical models with the fundamental theory of solid mechanics. The first numerical analysis was performed by Wolfs et al. using a commercial software ABAQUS, in which a hollow cylinder structure and a free wall layout are analyzed for structural failure of plastic collapse and elastic buckling, respectively [15,17,20]. This numerical model accurately reproduces the failure-deformation mode while a quantitative agreement with the experimental results could be improved. Inspired by this research, other research groups also used finite element method (FEM)-based approaches for analyses of 3DCP [10,35,37,40]. These studies are in accordance with the same fundamental principle but may use different failure criteria and different types of functions for defining material stiffness and strength evolution (i.e., linear or exponentially-decaying curing function). Although these FEM-based models are deemed more accurate than the analytical models, some issues remain. Rather, these models have not incorporated several relevant printing parameters, such as geometrical imperfections, non-uniform gravitational loading and material heterogeneity, which may affect the structural buildability. Particularly if a complex 3D geometry is analyzed, some localized damage may occur in layers other than the bottom one during actual printing, resulting in structural failure. In our previous research, localized damage and non-uniform gravitational loading have been introduced into the lattice model for buildability quantification. The published method using the load-unload method (LU) is able to reproduce the correct failure-deformation mode of plastic collapse, but a discrepancy with experimental results on critical printing height is observed [38]. This deviation might be attributed to the drawbacks of the load-unload method. More specifically, the deformed printing geometry and the non-proportional loading conditions occurring during 3D printing are not considered in the published model. Besides, using the load-unload method, the layer deformation of a printed object is calculated by the instantaneous material stiffness instead of being computed based on the time-dependent elastic modulus. Therefore, the model underestimates layer deformation. Additionally, the nonequilibrium force caused by the deformed printing geometry and localized damage is also not considered.

To achieve a quantitative agreement with experimental results, this research adopts the incremental method (IM) and updated Lagrangian method into the lattice model to quantify structural buildability for 3D concrete printing. In contrast to the published model which is based on the load-unload approach, the deformed printing geometry and non-proportional loading conditions can be considered through the newly proposed model. Furthermore, the nonequilibrium force via the generation of localized damage and the change of printing geometry is incorporated into numerical analyses of structural failure.

In this research, computational uniaxial compression tests are first simulated to study the impact of two algorithms (i.e., load-unload and

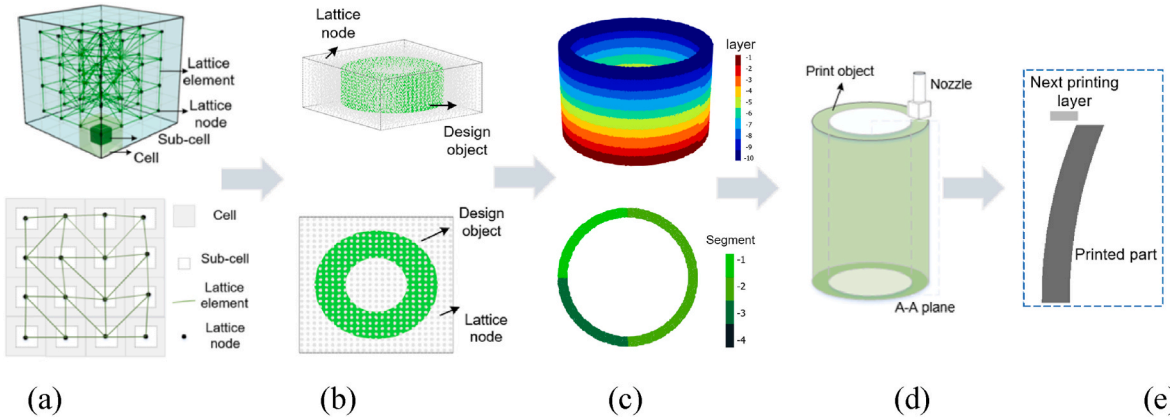

Fig. 1. Flowchart of lattice modelling on 3DCP (a) model generation (b) model establishment (c) layer division (d) structural analysis (e) structural failure criterion.

incremental) on numerical results including the peak load and the crack formation. Different results derived from the two methods indicate the significant influence of non-equilibrium force on the analysis. Then, the incremental method is adopted to assess the buildability of 3D concrete printing. Compared to published results using the load-unload method, better quantitative agreements with experiments are obtained using the incremental method and the reasons are also discussed.

2. Model description

2.1. Model introduction and applicability

In this study, the incremental method is introduced into the lattice model to predict the structural failure of plastic collapse. The impact of localized damage and deformed geometry is reflected in the form of a nonequilibrium force. Structural instability due to elastic buckling is not discussed herein and is a part of a related study [41]. The aim of that work is how to incorporate the geometric nonlinearity into lattice model and reproduce the asymmetric failure of buckling response without introducing initial geometrical imperfections. This proposed model applies to objects with a short printing time from minutes versus 1 h earlier, in which the printable materials are at a fresh stage. The model is based on the assumption of solid mechanics, and printed materials are considered in a solid-state. The fracture behavior of concrete in a fluid state is not simulated, despite the fact that it is a more important factor in the extrusion process. In addition, the viscous behavior is not considered, and the model in this study is therefore not capable of time-dependent deformation, namely early-stage shrinkage and creep. In relation to viscous deformation, relevant experimental data of fresh printing materials are required to provide input parameters for the numerical analysis. However, to the best of the authors' knowledge, no reliable published work reveals the mechanism behind these. This is therefore beyond the scope of the current work and will be addressed in the future.

2.2. Model generation and discretization

Fig. 1 gives an overview of pre-processing steps of 3DCP analysis, which includes model generation, discretization, material properties assignment, and failure criterion. Both the load-unload and incremental method share the same procedures on structural analysis, which can be divided into several steps and detailed information can be found from our previous work [38].

a) Model generation: A cubic domain is first built and divided into a number of cubic cells, in which sub-cells are generated. The lattice nodes are then randomly placed within these sub-cells through a pseudorandom number generator [42–44], allowing for mesh disorder. The cell size refers to the mesh resolution, and the length ratio between cell and sub-cell is defined as system randomness. Considering the low ratio of element length and height, the Timoshenko beams are adopted to consider shear deformation and discrete the printed object through Delaunay triangulation, as indicated in Fig. 1 (a).
b) Model establishment: The designed printing geometry is projected into the cubic domain for model establishment. For example, when generating a hollow cylinder structure, the hollow cylinder shape is projected into the cubic domain, as shown in Fig. 1 (b). Afterwards, the lattice nodes and elements inside the designed object are reserved while the rest are removed from the mesh system.
c) Layer division: While printing process, the non-uniform gravitational loading from successive printing layers leads to nonuniformity of structural deformation and generation of localized damage, causing fewer layers to be printed than otherwise expected. Therefore, modelling the non-uniform gravitational loading is essential to quantify structural buildability. In this study, each layer of the designed object is divided into several printing segments to mimic the continuous printing process, as indicated in Fig. 1 (c).
d) Nodal force calculation: In the lattice model, the nodal force allows for system gravitational loading. Considering the Delaunay triangulation is utilized to mesh system, the domain of a printed object is composed of a series of Voronoi cells. The volume of an individual Voronoi cell is computed to determine the magnitude of gravitational loading of each node, and the detailed procedures can be found in our previous research [38].
e) Element failure criterion: The lattice elements are assigned with tensile and compressive strength, which allows for material yielding. These material properties are calibrated via the green strength test simulations, as described in section 5.1. Once the element stress reaches the strength, it will be removed from the system, representing the localized damage during the printing process. Once an early-age fracture is initiated on the printed sample, the system is no longer in the elastic stage. Subjected to the non-uniform gravitational loading, the printing structure eventually fails with increasing plastic deformation.
f) Structural analysis: After model pre-processing, the buildability quantification will be performed through LU and IM, as indicated in Fig. 1 (d). The next printing segment is always placed on the initial/designed position rather than being adjusted based on deformed geometry, which is consistent with the actual printing process [15,27].
g) Structural failure criterion: In general, three typical failure modes can be found in 3D printing experiments, i.e., plastic collapse, elastic buckling, and combined failure mode, as reported in the literature [22,27,45]. All of them follow the same structural failure criterion, i.e., the next printing segment fails to be placed on the deformed

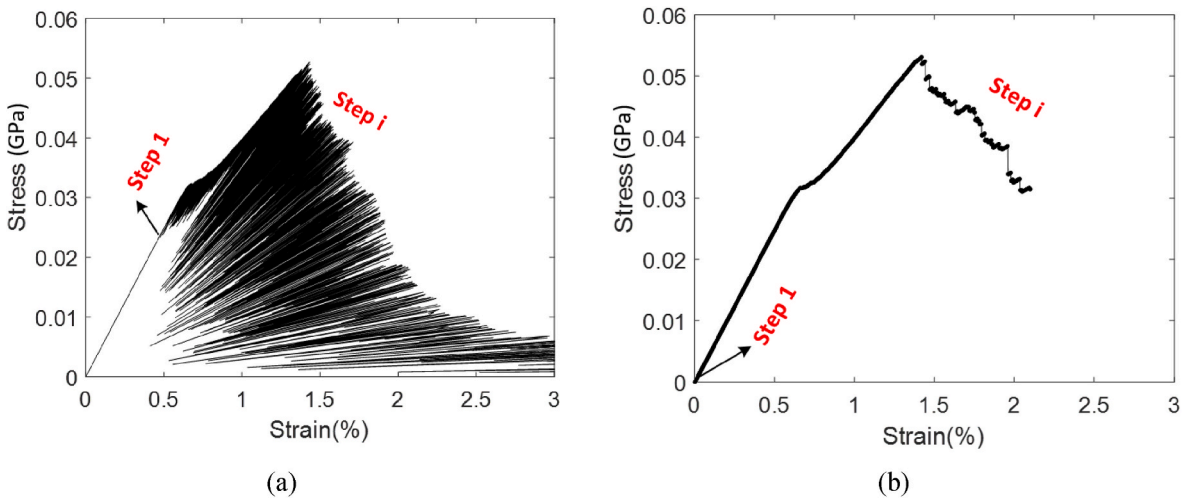

Fig. 2. Schematic diagram towards load-displacement curve using two methods (a) load-unload method (b) incremental method.

Table 2
Computational uniaxial compression tests with different material properties.

Model	Input parameters	Peak load		
		LU	IM	Difference
1	$E = 50$ KPa $f_t = 0.71$ KPa $f_c = 7.1$ KPa	14375 mN	13780 mN	4.32%
2	$E = 100$ KPa $f_t = 1.42$ KPa $f_c = 14.2$ KPa	28980 mN	27836 mN	4.11%
3	$E = 10$ GPa $f_t = 10$ MPa $f_c = 100$ KPa	202.77 kN	204.26 kN	−0.73%

*: E: elastic modulus; f_t: material tensile strength; f_c: material compressive strength; Difference =(IM-U)*100%/IM.

geometry. To describe the experimentally observed failure criterion, here the printing object is regarded as failed once the next printing segment fails to be placed on the printed system, which means that the offset between the design and actual position is at least equal to the width of the individual layer, as described in Fig. 1 (e). In general, this failure criterion accurately defines structural failure. However, when it comes to the printed structure with homogenous material properties, a uniform collapse of the printing structure can be achieved if the printing speed is low enough. In that situation, depending on this failure criterion, our model may overestimate the critical printing height. To avoid this unusual occurrence, we normally output the failure mode associated with the critical printing height to see when the printed structure exactly fails.

3. Recapitulation of load-unload and incremental methods

3.1. Overview

The modeling of fracture in cementitious materials has been under investigation over the past decades, two different non-iterative solving methods will be discussed in this study, i.e., the IM and LU.

The load-unload method removes the applied loading after each analysis step and then loads the system by a load increment which exactly results in one element break. This solution procedure repeats until a stopping criterion is reached. Fundamentally, the linear concept of the 'event-by-event' is preserved in the load-unload method; no iterations are utilized. Fig. 2 (a) shows a simulation result of a uniaxial compressive test using the load-unload method. Considering the analysis at each step is always conducted based on the initial statue, the assembling of the stiffness matrix is only done once through the entire analysis. This algorithm has been introduced into the lattice model for fracture analysis [46–49] due to its robustness and simplicity. Different from the LU, the IM considers the influence of deformed geometry and non-proportional loading problems.

For each analysis step, the incremental load is applied to the deformed system obtained from the last step. Subjected to the incremental load, some elements may break, resulting in disequilibrium force; and the stress redistribution is then conducted until a static equilibrium state is reached again; after that, the incremental load of the next analysis step is imposed on the system and the solution procedures continue until the final criterion is reached. Fig. 2 (b) shows an example of the response of a uniaxial compressive test derived using IM. This method is not only valid for non-proportional loading issues but also available for time-dependent problems.

There is however one drawback with IM, which is that the displacement that is used as feedback should be defined a priori. The displacement of the nodes that are chosen should always increase and no snap-backs can be simulated. As a consequence, this method is therefore size-dependent. In case of situations in which it is sure that the displacement always seems to increase, like in the case of early age material and 3D concrete printing, the method (IM) is valid. In case of large deformations in the material and progressive deformation IM is of course a much better option than LU, because node coordinates can be updated all the time and stress redistribution can be included in a better way by disequilibrium forces.

3.2. Case study: computational uniaxial compression test

During printing, the localized damage has a substantial impact on plastic collapse of structure failure. The primary goal of the case study is to highlight the difference between two numerical solutions (i.e., LU and IM) regarding the damage analysis through computational uniaxial compression tests. The investigated objectives involve the fracture performance and crack information, including the number of cracks, as well as their distribution and sequence. If the different damage information is obtained, these two methods may show different performance on buildability quantification of 3DCP. In contrast to the load-unload method, the incremental approach considers the influence of a number of parameters, including the deformed geometry, induced non-equilibrium force and non-proportional loading condition. Theoretically, it should better mimic the actual printing process.

First, computational uniaxial compression tests are performed to see how two approaches (i.e., LU and IM) affect numerical results including the load-displacement curve and fracture information. Three groups of input parameters are utilized, representative of concretes for different hardening times as shown in Table 2. All models are cylinder-shaped

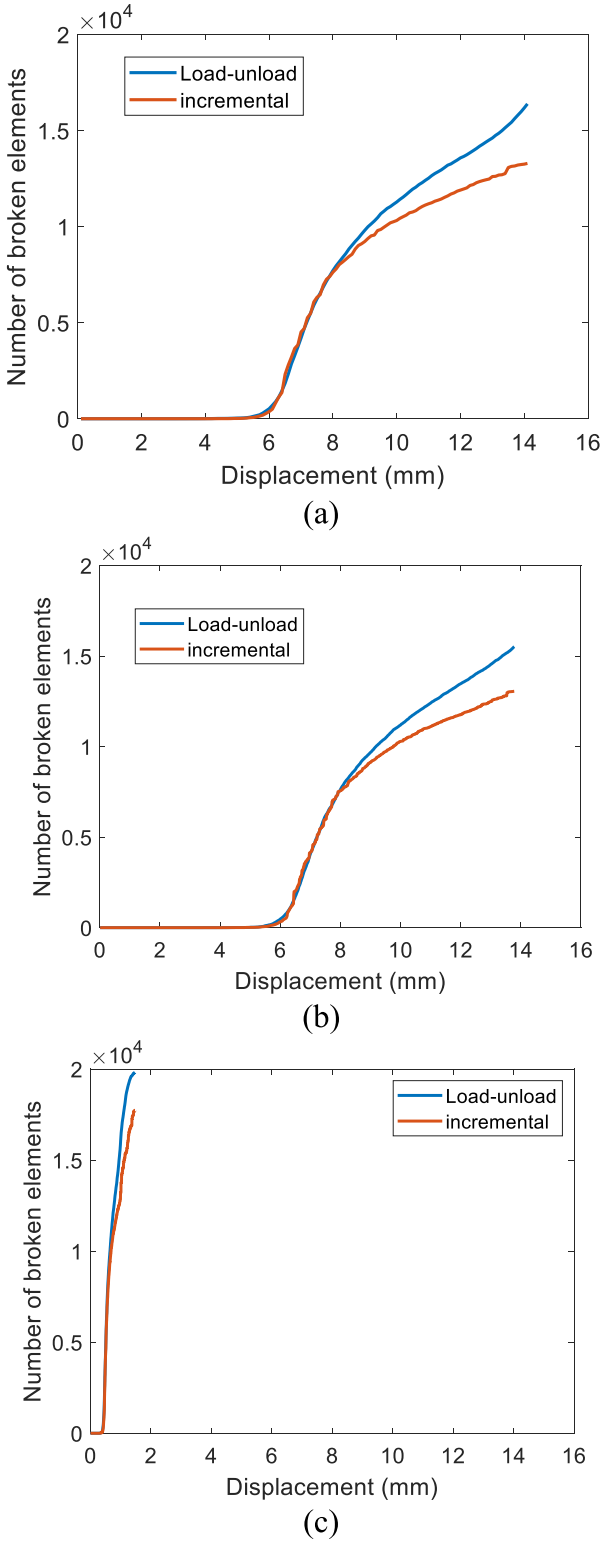

Fig. 3. Number of broken elements with displacement (a) model 1 (b) model 2 (c) model 3.

with the dimension of 70 mm diameter and 140 mm height.

There is a small difference in peak load for three models with different materials properties, as shown in Table 2. Model 3 with the lowest material properties generates the largest variance using these two methods (4.32%). Fig. 3 provides the number of broken elements with displacement using LU and IM analyses. Overall, these results show a discrepancy in the crack information obtained from two methods, which leads to the same results with the simulation from Eliáš, J. [50] (who considered hardened concrete). A further increase in the discrepancy in the number of broken elements can be found with increased displacement. These discrepancies are due to the impact of deformed geometry and the influence of the nonequilibrium force induced by the localized damage. This case study demonstrates the inclusion of nonequilibrium force and deformed geometry affects peak load and crack information, and the influence is obvious for early-age concrete.

4. Model methodology on 3D concrete printing

4.1. Load-unload method

In brief, the load-unload method applies the total gravitational load to the current printing system and computes the structural deformation based on the instantons material properties. After each analysis step, this load will be removed from the system. This solution method generally underestimates the structure deformation, resulting in an overestimated critical printing height. Furthermore, deformed geometry is not considered and the stress redistribution is also neglected. More detailed information about the numerical procedures can be found in Ref. [38].

4.2. Incremental analysis

In this study, an enhancement of the incremental method is proposed to simulate non-proportional loading characteristics and capture correct layer deformation based on the updated Lagrange approach.

4.2.1. Theoretical framework

Compared to load-unload approach, the incremental method applies the gravitational load in increments. In each step, the delate incremental displacement is computed to integrate the previous structural deformation for the total one. Thus, the layer deformation is a summation including a series of incremental displacements which should be computed based on the time-dependent material stiffness. Meanwhile, the delta displacement induced by the incremental load is also computed, altering the printed geometry. Thus, a stress distribution occurs, bringing an additional force to the printed system. Within this analysis step, this stress redistribution needs to be conducted until no further damage happen. In that way, at this time step, the stable stage is reached and the printing process proceeds.

4.2.2. Model implementation

The model implementation based on the incremental analysis can be divided into five branches: A, B, C, D, and E, as indicated in Fig. 4. The model initialization, fracture check, and structural failure criterion in 3DCP are identical to those in the previously published study using load-unload method [38]. The numerical solution and stress redistribution owing to deformed geometry and damage, on the other hand, are new.

4.2.2.1. Branch A: model initialization. After model establishment and discretization, numerical analyses of structural failure are conducted using the incremental method. The element stiffness and strength of printing segments are first computed based on corresponding properties of printing time to assemble the system stiffness matrix K.

4.2.2.2. Branch B: load increment. In each analysis step, the incremental load is the difference between the gravitational loading of printed segments and element force, which is affected by the generation of localized damage and change of printing geometry. Subjected to the disequilibrium force, a series of linear analyses are conducted to derive the incremental displacement, leading to the renewal of the internal force and the printing geometry. Here, the second-order Runge-Kutta method is adopted for solving the system of equations, and parallel computing is

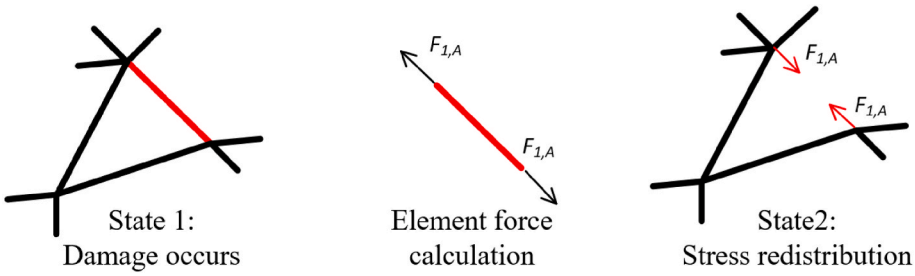

Fig. 4. A diagram for stress redistribution due to damage.

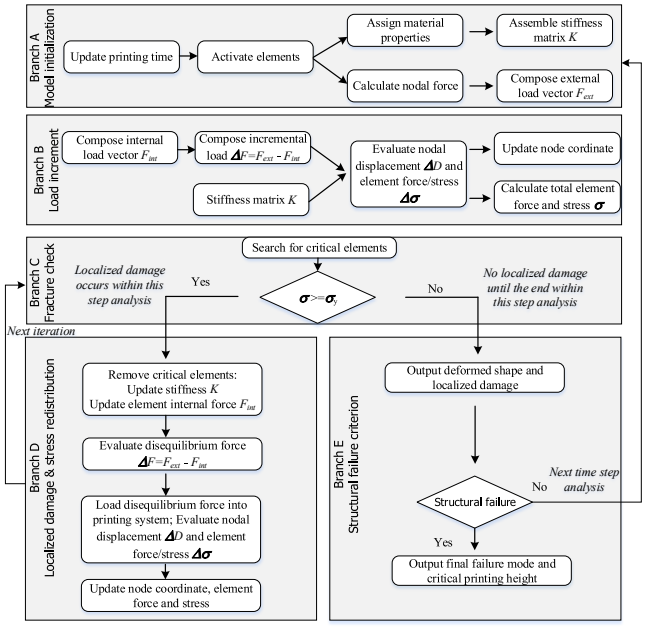

Fig. 5. Flowchart of the developed incremental algorithm on 3DCP.

used for computational efficiency.

4.2.2.3. Branch C: fracture check. Regarding the buildability quantification of 3DCP, the element removal mechanism is adopted to mimic the localized damage during the printing process. Once the material yield stress is reached, these elements will be marked as critical elements and removed from the system. For element failure criterion, the uniaxial force and bending moment is adopted for stress computation, as follows,

$$\sigma = \alpha_N \frac{F}{A} + \alpha_M \frac{\left(|M_i|, |M_j|\right)_{\max}}{W} \qquad (1)$$
$$\sigma_{yield} \leq \sigma$$

where, F and M refer to uniaxial force and bending moment in the local coordinate of an element; A is element cross-section and W stands for section modulus, both of them are the same for all elements; the coefficients α_N and α_M account for the influence of normal force and bending on element failure, and α_N equal to 1.0 [44,47,51,52] and α_M equal to 0.05 are generally adopted in agreement with the literature [44,51,53–56]. The σ_{yield} is the yield stress, which usually adopts the material tensile and compressive strength as default values [38].

4.2.2.4. Branch D: localized damage and stress redistribution. When removing critical elements from the system, the material stiffness and strength of these elements will be set to zero, thereby resulting in a disequilibrium force to the current printing system, as shown in Fig. 4. Subsequently, stress redistribution is then performed for another iteration. As soon as no damage occurs, the iterative computation of this step stops, indicating a stable stage is derived for the deformed printing geometry.

4.2.2.5. Branch E: structural failure criterion. After each analysis step, the structural failure criterion as described in section 2.1 is utilized to assess whether the printed object fails or not. Once the structural failure criterion is reached, the critical printing height will be determined; otherwise, the numerical analysis will continue until structural failure.

This algorithm is similar to the incremental sequentially linear analysis in which the applied load is kept in the system and the next reference load is added for the exact one element broken [57,58]. However, two points of difference should be noted: first, the geometry will be updated based on the derived incremental displacement after each iteration solution; second, more than one element is removed within one analysis step. These modifications are in accordance with the actual printing trials, in which the applied gravitational loading results in a deformed printing geometry and lots of localized damages. Through the incremental method, the effect of the disequilibrium force due to the occurrence of localized damage and change of printing geometry on buildability quantification can be investigated.

5. Numerical analyses

This section studies the impact of the nonequilibrium force caused by localized damage and deformed printing geometry on the structural failure of plastic collapse for 3D concrete printing using the lattice model with the incremental solution. The effect of disequilibrium force on buildability quantification is studied through the comparison with previously published numerical results using the load-unload method [38]; and model performance on 3D printing analysis will be evaluated compared to the experimental results in the literature [15,27].

For buildability quantification, computational uniaxial compression tests are first conducted to calibrate material properties, including material stiffness and strength. Structural analyses of plastic collapse are then employed to assess when and how printed objects fail. Several failure-based characterizations, consisting of failure-deformation mode, critical printing height, and localized damage, are adopted to evaluate the prediction performance through load-unload and incremental methods for 3DCP.

5.1. Model calibration

This section discusses model calibration to derive age-dependent stiffness and strength of fresh, 3D printing materials. Herein, the computational uniaxial compression tests from the literature [15,27] are performed using two types of printing materials, with multiple measured ages spanning from 0 to approximately 90 min. Noted that the $t = 0$ is defined as the earliest time point with the possibility of starting the test, and approximately 5 min after material casting [15]. Specifically, material A is employed for hollow cylinder structure while square layout uses material B for the structural build-up of 3DCP [15,27].

A cylinder geometry with a diameter equal to 70 mm and height

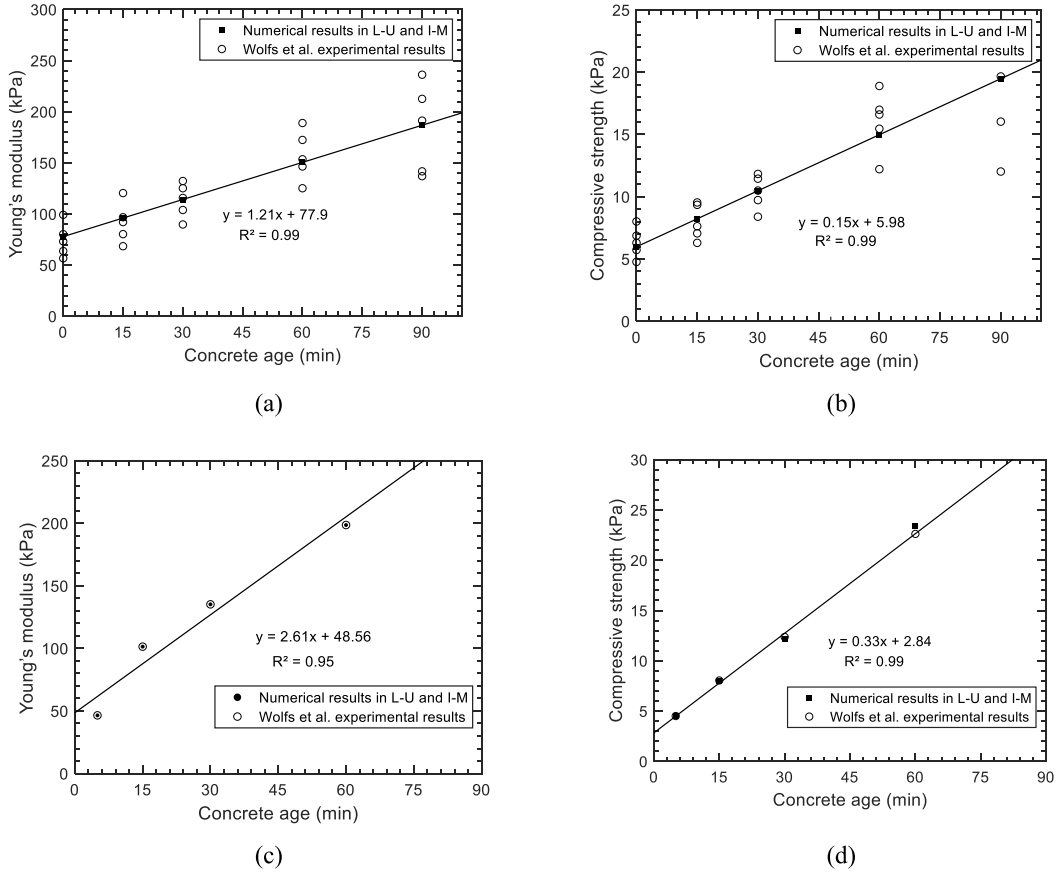

Fig. 6. Compressive strength and Young's modulus development from experimental results and lattice model, with concrete age 0–90 min.

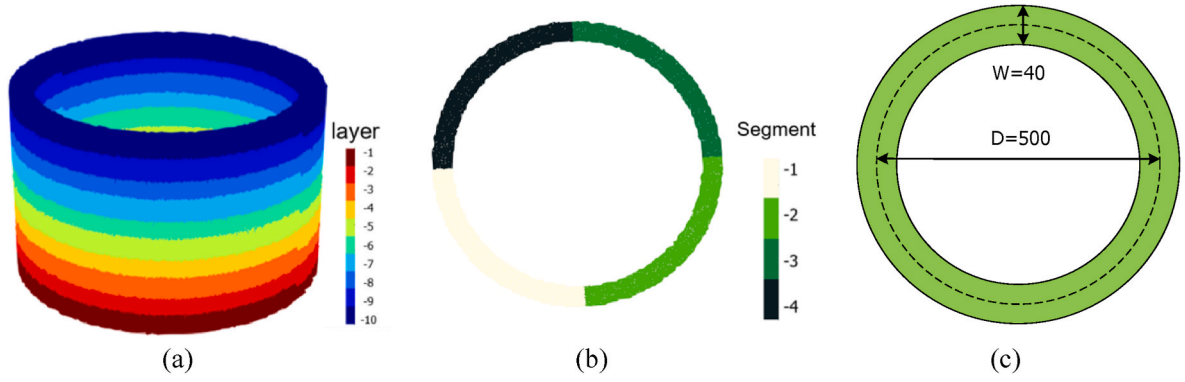

Fig. 7. Dimensions of cylinder structure for 3d concrete printing (a) layers of hollow cylinder structure (b) single layer division (c) dimensions of the printed object.

equal to 140 mm in accordance with the experimental sample in the literature is used to calibrate transient material properties [15,27]. This numerical model with a mesh resolution of 5 mm consists of 30614 Timoshenko beams connected by 4317 lattice nodes through Delaunay triangulation. The computational uniaxial compression tests are conducted under the boundary condition without friction, corresponding with friction minimization set in actual tests [15]. The model calibration is conducted using LU and IM, respectively. For the element failure criterion, the yield stress in the compressive state is assumed as 10 times higher than the tensile; this hypothesis is generally available to hardened cementitious materials and perhaps needs to be adjusted based on future experimental insights in 3D printable fresh materials. The detailed calibration procedures can be found in our published research [38,44]. During the calibration process, the time-dependent compressive strength and Young's modulus computed from the green strength test are the targets of the lattice simulation. The numerical results derived from the computational uniaxial compression test are shown in Fig. 5 along with test data. The relevant material properties towards lattice elements are what we want to get from the calibration process, which is adopted as input parameters for buildability quantification. Eqs (2)–(5) mathematically describe time-dependent Young's modulus and compressive strength of the lattice elements using linear functions. A linear relation seems valid at very early age, although at later age the development will slow down with time. Note that there are some differences in terms of material properties between load-unload and incremental methods. This is because of the combined effect caused by

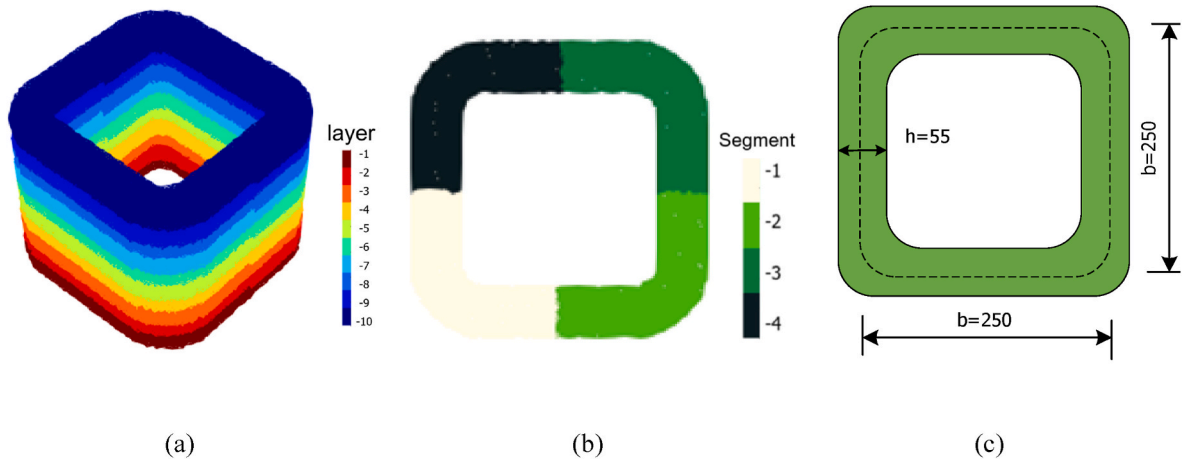

Fig. 8. Dimensions of square structure for 3D concrete printing (a) layers of square structure (b) single layer division (c) dimensions of a square layout.

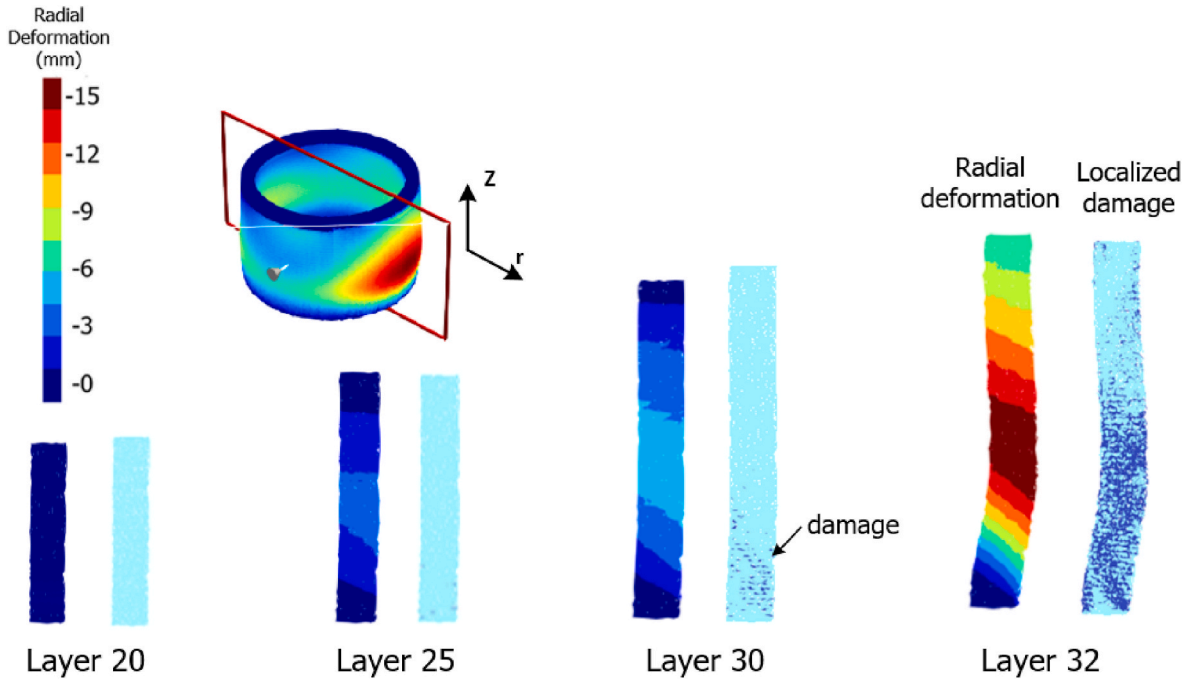

Fig. 9. Lattice model results deformed shape and occurrence of localized damage for hollow cylinder structure using the incremental method.

localized damage and deformed geometry, as explained in Section 3.2.

$$E^{A,\ LU}(t) = 77.9 + 1.21{\cdot}t \qquad f_c^{A,LU}(t) = 10.96 + 0.27{\cdot}t \tag{2}$$

$$E^{B,LU}(t) = 48.56 + 2.61{\cdot}t \qquad f_c^{B,LU}(t) = 5.2 + 0.6{\cdot}t \tag{3}$$

$$E^{A,\ IM}(t) = 77.9 + 1.21{\cdot}t \qquad f_c^{A,IM}(t) = 12.02 + 0.28{\cdot}t \tag{4}$$

$$E^{B,IM}(t) = 48.56 + 2.61{\cdot}t \qquad f_c^{B,IM}(t) = 4.63 + 0.75{\cdot}t \tag{5}$$

where t is defined as printing time; E is Young's modulus of lattice elements, determining elastic deformation within each time frame during the printing process; f_c represents material compressive strength, codetermining the localized damage together with tensile strength; two superscripts A and B refer to different types of printing materials; LU and IM refer to load-unload and incremental approach, respectively.

5.2. Model validation

5.2.1. Hollow cylinder structure

The hollow cylinder structure with 500 mm diameter, 40 mm thickness, and 10 mm layer height (as shown in Fig. 6), is employed for buildability quantification during the printing process, which is in accordance with the printing trials in the literature [15]. This numerical analysis adopts high friction as the boundary condition and divides each layer into 4 printing segments to mimic non-uniform gravitational loading due to the sequential printing process in actual trials, see Fig. 6 (b). To remove mesh size influence, 5 mm mesh resolution is utilized in this simulation. Each layer composes of about 5000 lattice nodes connected by around 360,000 lattice beams. The nodal force is codetermined by Voronoi volume and material density, which is around 2100 kg/m^3 derived from experimental data [15].

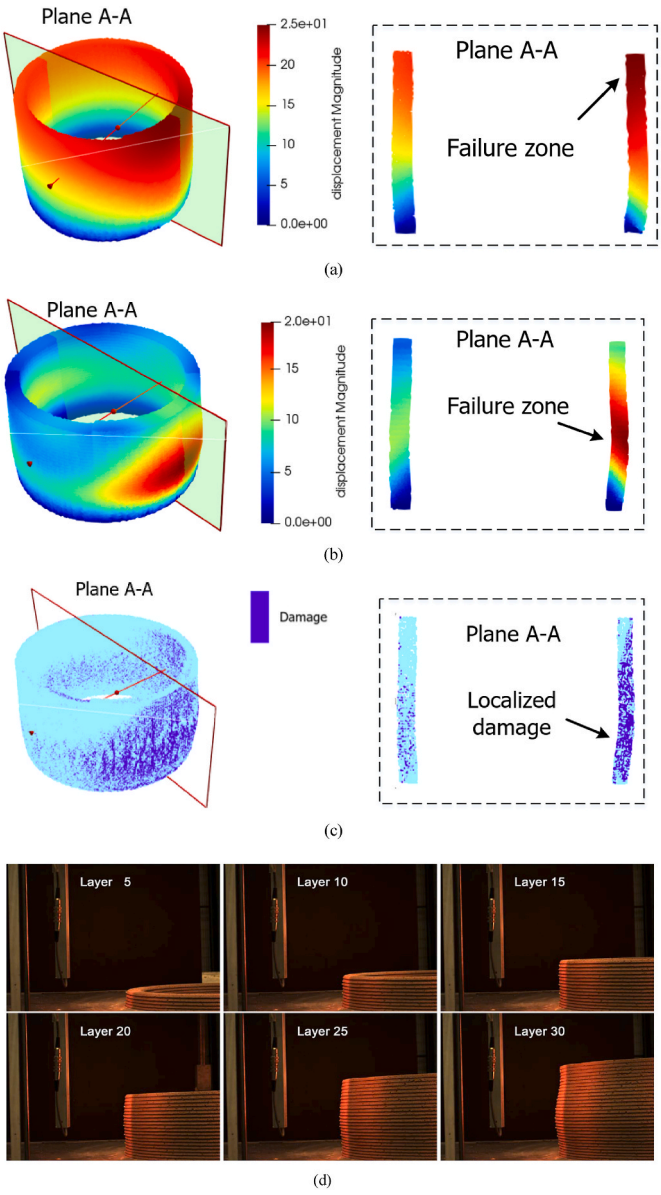

Fig. 10. Final-deformation mode of hollow cylinder structure (a) load-unload method (41st layer) [[38]] (b)incremental method: failure deformation (32nd layer) (the structural deformation is magnified to see. Unit: mm) (c)incremental method: localized damage (32nd layer) (d) experimental results. Reproduced from Ref. [15]. Copyright 2018, Elsevier.

5.2.2. *Large square*

Considering the fact that cylindrical geometry is sensitive to imperfections for structural analysis [59,60], a square layout is therefore added for model validation. The size information of the square structure is listed in Fig. 7, i.e., layer height of 10 mm, and a radial corner of 50 mm. Regarding model discretization, the same mesh resolution (5 mm) is employed and each layer of the square layout includes around 4300 lattice nodes and 31,000 lattice elements. The nodal force, characterized by Voronoi volume and material density of 2100 kg/m^3, is comparable to the numerical analysis of hollow cylinder structure, as well as the boundary condition and layer division.

In relation to printing velocity, the interval time between two layers is 0.31 min and 0.16 min for hollow cylinder and square structure correlated with printing speed in actual tests. Lattice modeling of plastic collapse is carried out through two steps. The first step concerns the development of material properties, in which new printing elements are activated and material stiffness and strength develop following a linear function, as mathematically described from eqs (2)–(5). For instance, when assuming the interval time between two segments is 0.62 min, the total printing time reaches 3.1 min after deposition of 5 printing segments. Consequently, the first printing segment is assigned to corresponding properties of 0.31 min age while the 5th segment has the properties of 0 min. The second step concerns structural analyses during the printing process, as explained in section 4, where the two algorithms, namely, LU and IM, are employed for buildability quantification. The numerical analysis is performed until the structural failure criterion is reached, i.e., the next printing segment fails to be placed on deformed geometry.

In 3DCP, there is a standoff distance between the printed structure and nozzle in 3DCP. Depending on this distance, two subcategories of printing processes for extrusion-based materials can be distinguished. If the standoff distance is positive, the printed materials are extruded from the nozzle and placed on the deformed structure. In that case, the gravitational load due to the printed segments mainly affect the structure deformation. Once this distance is negative, the newly printed segments are extruded to the printed structure under the gravitational load and extrusion pressure. This extrusion pressure significantly determines the structure deformation. This pressure must be considered in the model when quantifying the structure buildability in such an instance. In these two printing experiments, the new printing segments are placed on the deformed structure without pressure force, as described in the literature [15,27]. As a result, we did not include this sort of force in our model for quantifying buildability.

5.3. *Numerical results*

In 3DCP, failure modes, critical printing height, and structural deformation are common experimentally derived parameters for buildability quantification in 3DCP. In this section, modelling the printed structures reproduces the correct failure mode qualitatively, much like visual inspection. The critical printing height, radial deformation, and structure deformation are provided for quantitative comparison.

Fig. 8 shows radial deformation and occurrence of localized damage during printing process, showing that a growing number of printing layers result in a larger radial deformation. Meanwhile, increasing amount of damage can also be observed from the deformed printing geometry. This is attributed to the non-uniform gravitational loading from successive printing segments, and due to the disequilibrium force caused by the generation of localized damage and the change of printing geometry. To be specific, a new printing segment is placed on the deformed printing system, resulting in more localized damage occurrence and a larger structural deformation. This influence may, in turn, affect the non-uniform state of stress which can result in structural collapse. In the end, a majority of lattice elements in the bottom layers break (as shown in Fig. 9), leading to structural failure of plastic collapse. Concerning the system deformation (defined as the square root computed through the displacements in three translations, i.e., sqrt (x^2+y^2+z^2)), the zone with maximal deformation derived from the load-unload method is close to the top area, as shown in Fig. 9 (a). However, the incremental method predicts structural maximum deformation near the middle of the cylinder height, as shown in Fig. 9 (b). Meanwhile, numerous broken elements also can be observed due to large radial deformation in Fig. 9 (c). The experimental result from the literature (Fig. 9 (d)) indicates that the incremental method better reproduces the failure-deformation mode [15]. In relation to the generation of localized damage, Fig. 10 (a) indicates that the number of broken elements derived from increment methods is higher than that obtained through the load-unload solution under the same gravitational loading condition. Thus, the incremental method (IM) predicts a lower critical printing layer than the load-unload method (LU). Eventually, the printing object fails due to material yielding.

Fig. 10 (b) describes the generation of localized damage versus the

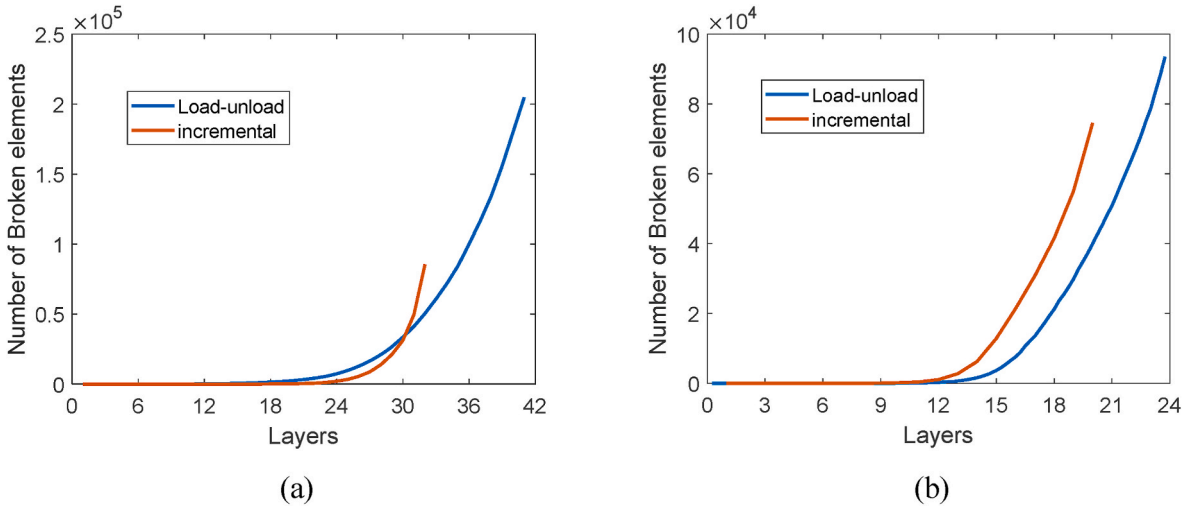

Fig. 11. Generation of localized damage during the printing process (a) hollow cylinder structure (b) square structure.

printing layers for the large square structure. Compared to the load-unload method, more broken elements are found using the incremental solution, which is attributed to the inclusion of disequilibrium force and updating of nodal coordinates with increasing deformation as shown in Fig. 11. Fig. 12 provides the failure-deformation mode and the occurrence of localized damage of the square layout using the two algorithms. Although two different approaches predict different failure zones with maximal deformation, the failure-deformation modes, characterized by localized damage and excessive deformation, are comparable. Eventually, numerous lattice elements within the bottom layers break, leading to the structural failure of plastic collapse, as illustrated in Fig. 12 (c). This failure mode with an obvious cross-section increasing on the bottom layers can be easily observed from Fig. 12 (b), which is in accordance with the experimental findings as shown in Fig. 12 (d) [27].

Table 3 lists a series of failure characterizations, consisting of critical printing height, maximum radial deformation, and corresponding z position among lattice model using load-unload [38] and incremental method, FEM-based model from Wolfs et al. [15], and experimental results [15,27]. Differences are obtained between the experimental data and the different simulation methods. These differences are expected also because of variation of material properties and circumstances when performing the experiments. The most important, however, is to conclude that the IM method predicts the same failure mechanism as in the experiment and therefore it seems better than the LU method.

6. Discussion

When comparing the predicted critical heights from the lattice model using the two approaches, the numerical results indicate that the incremental method predicts a lower critical printing height than the load-unload method, which is ascribed to consideration of deformed geometry and disequilibrium force. Specifically, the total deformation of the printing structure is determined by the transient material stiffness using the load-unload method. However, the layer deformation is a summation including a series of incremental displacements which should be computed based on the time-dependent material stiffness. Besides, based on the deformed printing geometry, the disequilibrium force induced by the geometry change and damage generation can be included using the incremental solution. The localized damage has significant influence on plastic collapse during the printing process. Considering that the lattice model with incremental approach reproduces the correct failure-deformation mode as well as quantitative agreement result with experimental data, it can be considered as a more precise method for buildability quantification of 3DCP.

However, compared to experimental results, some discrepancy can also be found. The incremental solution underestimates printing height of the hollow cylinder structure while the opposite is observed for the square layout. This difference is attributed to exclusion of geometric imperfection and possible underestimation of material properties used as input in the model.

The development of material properties is obtained using the green strength test, in which printable materials are actually cast and therefore undergo a compaction process [15,27]. This process may result in a low early-stage material stiffness and strength with the time frame of the first 30 min [20]. Furthermore, viscoelastic behavior like creep and relaxation is not considered. This will both be present in the green strength testing, but also during printing. Consequently, the critical printing height is underestimated derived using these material properties. To obtain more reliable input parameters, some improvements on the material test are recommended without the compaction process may be needed, however, this is beyond the scope of current research.

The underestimation of the number of critical layers can be found from square geometry while the opposite tendency is also found for hollow cylinder structure, which can be attributed to another factor, namely, presence of geometric imperfection induced by extrusion and printing process. For 3DCP, there are two types of imperfections may be generated during the printing process; the first one comes from the manufacturing process given the fact that printable materials cannot be smoothly extruded from the nozzle; the second one is localized damage. The model presented in this chapter only allows for localized damage that is generated due to the loading conditions but neglects imperfections resulting from the printing procedure. The critical printing height is possible to be overestimated using the lattice model with the incremental solution, especially for hollow cylinder structure instead of the square layout. This is because the cylinder geometry is much more sensitive to imperfections compared with the square structure [26,27]. Once the imperfection like air pore and layer tearing and development of shrinkage stresses during the manufacturing process are considered, a better quantitative agreement with experimental data may be achieved.

7. Conclusions

This research investigates the influence of disequilibrium force due to localized damage and deformed printing geometry on the structural failure of plastic collapse by comparing load-unload and incremental methods through the lattice model. A series of novel insights and conclusions can be reached as below:

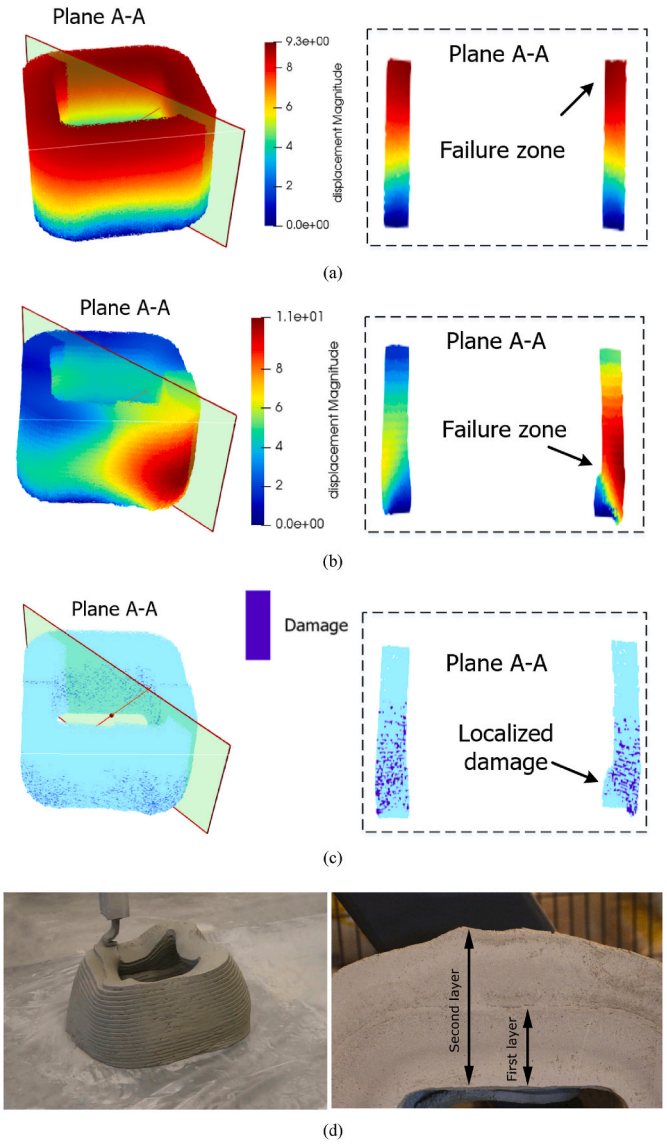

Fig. 12. Final-deformation mode of square structure (a) load-unload method (24th layer) [38] (b) incremental method: failure deformation (20th layer) (the structural deformation is magnified to see. Unit: mm) (c) incremental method: localized damage (20th layer) (d) experimental results. Reproduced from Ref. [27]. Copyright 2020, Elsevier.

1. Compared to the load-unload method, the incremental method considers disequilibrium force via the generation of localized damage and the change of printing geometry. For the computational uniaxial compression test, the inclusion of this kind of force results in different peak load and crack information, and the influence is obvious for early-age cement-based material.
2. For 3D concrete printing analysis, the load-unload method underestimates the layer deformation based on instantaneous material stiffness. The correct layer deformation is a summation including a series of incremental displacements which should be computed based on the time-dependent material stiffness. The lattice model with an incremental approach is considered an accurate method to capture structural deformation during the printing process.
3. In contrast to the published load-unload method, the incremental approach reproduces more accurate failure-deformation mode as well as quantitively agreement results with experimental data. This is due to the consideration of deformed geometry and the inclusion of nonequilibrium force.

Table 3
Overview of failure-deformation results of the cylinder and square structures including critical printing height, radial deformation, and corresponding height.

Object	Parameter		Value	Relative error
Hollow cylinder	Critical printing height	Experiment	29 layers	–
		Load-unload method	41 layers	41.38%
		Incremental method	32 layers	10.34%
		Wolfs et al.	46 layers	58.62%
	Max radial deformation (mm)	Experiment	15.3 mm	–
		Load-unload method	14.42 mm	5.75%
		Incremental method	14.9 mm	2.61%
		Wolfs et al.	13.89 mm	10.87%
	Z position of max radial deformation (mm)	Experiment	114.7 mm	–
		Load-unload method	115.36 mm	<1%
		Incremental method	128.09 mm	11.67%
		Wolfs et al.	115.8 mm	1%
Square	Critical printing height	Experiment	218.5 mm	–
		Load-unload method	240 mm	9.84%
		Incremental method	200 mm	−8.47%

4. A small deviation between lattice modeling using the incremental method and the experimental results can be found. This is likely because of the underestimated material properties from testing, and because of disregarding the impact of geometrical imperfections generated during the extrusion and printing process.

Based on the numerical results, it can be concluded the lattice model with the incremental method can be considered as a more approximate method for buildability quantification of 3DCP. Through the incremental method, in the next research, several time-dependent factors such as creep and shrinkage will be incorporated into the lattice model to study their impact on buildability quantification.

Declaration of competing interest

The authors declare that they have no known competing financial interests or personal relationships that could have appeared to influence the work reported in this paper.

Data availability

Data will be made available on request.

Acknowledgements

Ze Chang and Minfei Liang would like to acknowledge the funding supported by China Scholarship Council under grant numbers 201806060129 and 202007000027. Branko Šavija and Yading Xu acknowledge the financial support of the European Research Council (ERC) within the framework of the ERC Starting Grant Project “Auxetic Cementitious Composites by 3D printing (ACC-3D)”, Grant Agreement Number 101041342. The authors are grateful to Lu Cheng and Chenjie Yu from Delft University of Technology for the useful discussions on the incremental method, their support is gratefully acknowledged.

References

[1] J. Pegna, Exploratory investigation of solid freeform construction, Autom. ConStruct. 5 (5) (1997) 427–437.
[2] F. Bester, M. van den Heever, J. Kruger, G. van Zijl, Reinforcing digitally fabricated concrete: a systems approach review, Addit. Manuf. 37 (2020), 101737.
[3] A. Perrot, A. Pierre, V. Nerella, R. Wolfs, E. Keita, S. Nair, N. Neithalath, N. Roussel, Mechtcherine, from analytical methods to numerical simulations: a process engineering toolbox for 3D concrete printing, Cement Concr. Compos. 122 (2021), 104164.
[4] C. Yang, Y. Kim, S. Ryu, G.X. Gu, Prediction of composite microstructure stress-strain curves using convolutional neural networks, Mater. Des. 189 (2020), 108509.
[5] G.H.A. Ting, Y.W.D. Tay, M.J. Tan, Experimental measurement on the effects of recycled glass cullets as aggregates for construction 3D printing, J. Clean. Prod. 300 (2021), 126919.
[6] R.A. Buswell, W.L. da Silva, F.P. Bos, H. Schipper, D. Lowke, N. Hack, H. Kloft, V. Mechtcherine, T. Wangler, N. Roussel, A process classification framework for defining and describing Digital Fabrication with Concrete, Cement Concr. Res. 134 (2020), 106068.
[7] T.A. Salet, Z.Y. Ahmed, F.P. Bos, H.L. Laagland, Design of a 3D printed concrete bridge by testing, Virtual Phys. Prototyp. 13 (3) (2018) 222–236.
[8] S. Hou, Z. Duan, J. Xiao, J. Ye, A review of 3D printed concrete: performance requirements, testing measurements and mix design, Construct. Build. Mater. (2020), 121745.
[9] T.T. Le, S.A. Austin, S. Lim, R.A. Buswell, A.G.F. Gibb, T. Thorpe, Mix design and fresh properties for high-performance printing concrete, Mater. Struct. 45 (8) (2012) 1221–1232.
[10] R. Jayathilakage, P. Rajeev, J. Sanjayan, Yield stress criteria to assess the buildability of 3D concrete printing, Construct. Build. Mater. 240 (2020), 117989.
[11] R. Jayathilakage, J. Sanjayan, P. Rajeev, Direct shear test for the assessment of rheological parameters of concrete for 3D printing applications, Mater. Struct. 52 (1) (2019) 1–13.
[12] H. Jeong, S.-J. Han, S.-H. Choi, Y.J. Lee, S.T. Yi, K.S. Kim, Rheological property criteria for buildable 3D printing concrete, Materials 12 (4) (2019) 657.
[13] N. Roussel, Rheological requirements for printable concretes, Cement Concr. Res. 112 (2018) 76–85.
[14] R. Jayathilakage, P. Rajeev, J. Sanjayan, Extrusion rheometer for 3D concrete printing, Cement Concr. Compos. 121 (2021), 104075.
[15] R. Wolfs, F. Bos, T. Salet, Early age mechanical behaviour of 3D printed concrete: numerical modelling and experimental testing, Cement Concr. Res. 106 (2018) 103–116.
[16] V. Mechtcherine, F.P. Bos, A. Perrot, W.L. da Silva, V. Nerella, S. Fataei, R.J. Wolfs, M. Sonebi, N. Roussel, Extrusion-based additive manufacturing with cement-based materials–Production steps, processes, and their underlying physics: a review, Cement Concr. Res. 132 (2020), 106037.
[17] R. Wolfs, A. Suiker, Structural failure during extrusion-based 3D printing processes, Int. J. Adv. Manuf. Technol. 104 (1–4) (2019) 565–584.
[18] B. Panda, N. Mohamed, N. Ahamed, S.C. Paul, G. Bhagath Singh, M.J. Tan, B. Šavija, The effect of material fresh properties and process parameters on buildability and interlayer adhesion of 3D printed concrete, Materials 12 (13) (2019) 2149.
[19] B. Panda, J.H. Lim, M.J. Tan, Mechanical properties and deformation behaviour of early age concrete in the context of digital construction, Compos. B Eng. 165 (2019) 563–571.
[20] R. Wolfs, F. Bos, T.J.C. Salet, Triaxial compression testing on early age concrete for numerical analysis of 3D concrete printing, Cement Concr. Compos. 104 (2019), 103344.
[21] A. Rahul, M. Santhanam, H. Meena, Z. Ghani, 3D printable concrete: mixture design and test methods, Cement Concr. Compos. 97 (2019) 13–23.
[22] J. Kruger, S. Zeranka, G. van Zijl, 3D concrete printing: a lower bound analytical model for buildability performance quantification, Autom. ConStruct. 106 (2019), 102904.
[23] J. Kruger, S. Zeranka, G. van Zijl, Quantifying Constructability Performance of 3D Concrete Printing via Rheology-Based Analytical Models, Rheology and Processing of Construction Materials, Springer, 2019, pp. 400–408.
[24] A. Perrot, D. Rangeard, A. Pierre, Structural built-up of cement-based materials used for 3D-printing extrusion techniques, Mater. Struct. 49 (4) (2016) 1213–1220.
[25] T. Wangler, E. Lloret, L. Reiter, N. Hack, F. Gramazio, M. Kohler, M. Bernhard, B. Dillenburger, J. Buchli, N. Roussel, Digital concrete: opportunities and challenges, RILEM Technical Letters 1 (2016) 67–75.
[26] A.S.J. Suiker, Mechanical performance of wall structures in 3D printing processes: theory, design tools and experiments, Int. J. Mech. Sci. 137 (2018) 145–170.
[27] A.S. Suiker, R.J. Wolfs, S.M. Lucas, T.A. Salet, Elastic buckling and plastic collapse during 3D concrete printing, Cement Concr. Res. 135 (2020), 106016.
[28] R. Comminal, W.R.L. da Silva, T.J. Andersen, H. Stang, J. Spangenberg, Modelling of 3D concrete printing based on computational fluid dynamics, Cement Concr. Res. 138 (2020), 106256.
[29] M.P. Serdeczny, R. Comminal, D.B. Pedersen, J. Spangenberg, Numerical simulations of the mesostructure formation in material extrusion additive manufacturing, Addit. Manuf. 28 (2019) 419–429.
[30] M.T. Mollah, R. Comminal, M.P. Serdeczny, D.B. Pedersen, J. Spangenberg, Stability and Deformations of Deposited Layers in Material Extrusion Additive Manufacturing, Additive Manufacturing, 2021, 102193.
[31] M. Chen, L. Li, Y. Zheng, P. Zhao, L. Lu, X. Cheng, Rheological and mechanical properties of admixtures modified 3D printing sulphoaluminate cementitious materials, Construct. Build. Mater. 189 (2018) 601–611.
[32] F.A. Cardoso, V.M. John, R.G. Pileggi, Rheological behavior of mortars under different squeezing rates, Cement Concr. Res. 39 (9) (2009) 748–753.
[33] T. Di Carlo, B. Khoshnevis, A. Carlson, Experimental and Numerical Techniques to Characterize Structural Properties of Fresh Concrete, ASME International Mechanical Engineering Congress and Exposition, American Society of Mechanical Engineers, 2013, V009T10A062.
[34] J. Kruger, S. Zeranka, G.J.C. van Zijl, B. Materials, An ab initio approach for thixotropy characterisation of (nanoparticle-infused), 3D printable concrete 224 (2019) 372–386.
[35] T. Ooms, G. Vantyghem, R. Van Coile, W. De Corte, A parametric modelling strategy for the numerical simulation of 3D concrete printing with complex geometries, Addit. Manuf. 38 (2021), 101743.
[36] G. Vantyghem, T. Ooms, W. De Corte, VoxelPrint: a Grasshopper plug-in for voxel-based numerical simulation of concrete printing, Autom. ConStruct. 122 (2021), 103469.
[37] M. Mengesha, A. Schmidt, L. Göbel, T. Lahmer, Numerical modeling of an extrusion-based 3D concrete printing process considering a spatially varying pseudo-density approach, in: RILEM International Conference on Concrete and Digital Fabrication, Springer, 2020, pp. 323–332.
[38] Z. Chang, Y. Xu, Y. Chen, Y. Gan, E. Schlangen, B. Šavija, A discrete lattice model for assessment of buildability performance of 3D-printed concrete, Comput. Aided Civ. Infrastruct. Eng. 36 (5) (2021) 638–655.
[39] Z. Chang, E. Schlangen, B. Šavija, Extended lattice model to simulate the printing process of 3D printed cementitious materials, in: RILEM International Conference on Concrete and Digital Fabrication, Springer, 2020, pp. 814–823.
[40] G. Vantyghem, T. Ooms, W. De Corte, FEM Modelling Techniques for Simulation of 3D Concrete Printing, 2020 arXiv preprint arXiv:.06907.
[41] Z. Chang, H. Zhang, M. Liang, et al., Numerical simulation of elastic buckling in 3D concrete printing using the lattice model with geometric nonlinearity, Automation in Construction 142 (2022) 104485.
[42] H. Zhang, B. Šavija, E. Schlangen, Combined experimental and numerical study on micro-cube indentation splitting test of cement paste, Eng. Fract. Mech. 199 (2018) 773–786.
[43] H. Zhang, Y. Xu, Y. Gan, E. Schlangen, B. Šavija, Experimentally validated meso-scale fracture modelling of mortar using output from micromechanical models, Cement Concr. Compos. 110 (2020), 103567.
[44] Z. Chang, H. Zhang, E. Schlangen, B. Šavija, Lattice fracture model for concrete fracture revisited: calibration and validation, Appl. Sci. 10 (14) (2020) 4822.
[45] J. Kruger, S. Cho, S. Zeranka, C. Viljoen, G. van Zijl, 3D concrete printer parameter optimisation for high rate digital construction avoiding plastic collapse, Compos. B Eng. 183 (2019), 107660.
[46] H.J. Herrmann, A. Hansen, S. Roux, Fracture of disordered, elastic lattices in two dimensions, Phys. Rev. B 39 (1) (1989) 637.
[47] E. Schlangen, E.J. Garboczi, Fracture simulations of concrete using lattice models: computational aspects, Eng. Fract. Mech. 57 (2–3) (1997) 319–332.
[48] Z. Pan, R. Ma, D. Wang, A. Chen, A review of lattice type model in fracture mechanics: theory, applications, and perspectives, Eng. Fract. Mech. 190 (2018) 382–409.
[49] E. Schlangen, J.G.M. Van Mier, Simple lattice model for numerical simulation of fracture of concrete materials and structures, Mater. Struct. 25 (9) (1992) 534–542.
[50] J. Eliáš, Generalization of load–unload and force-release sequentially linear methods, Int. J. Damage Mech. 24 (2) (2015) 279–293.
[51] E. Schlangen, Experimental and Numerical Analysis of Fracture Processes in Concrete, Delft University of Technology, Delft, The Netherlands, 1993.
[52] N. Jiang, H. Zhang, Z. Chang, E. Schlangen, Z. Ge, B. Šavija, Discrete lattice fracture modelling of hydrated cement paste under uniaxial compression at micro-scale, Construct. Build. Mater. 263 (2020), 120153.
[53] M. Vassaux, F. Ragueneau, B. Richard, A. Millard, Compressive behavior of a lattice discrete element model for quasi-brittle materials, Computational Modelling of Concrete Structures 1 (2014) 335–344.
[54] Z. Qian, Multiscale Modeling of Fracture Processes in Cementitious Materials, Delft University of Technology, Delft, The Netherlands, 2012.
[55] Z. Qian, E. Schlangen, G. Ye, K. van Breugel, Modeling framework for fracture in multiscale cement-based material structures, Materials 10 (6) (2017).
[56] H. Zhang, B. Šavija, S. Chaves Figueiredo, M. Lukovic, E. Schlangen, Microscale testing and modelling of cement paste as basis for multi-scale modelling, Materials 9 (11) (2016).
[57] C. Yu, P. Hoogenboom, J. Rots, Extension of incremental sequentially linear analysis to geometrical non-linearity with indirect displacement control, Eng. Struct. 229 (2021), 111562.
[58] J. Eliáš, P. Frantík, M. Vořechovský, Improved sequentially linear solution procedure, Eng. Fract. Mech. 77 (12) (2010) 2263–2276.
[59] W.T. Koiter, On the Stability of Elastic Equilibrium, National Aeronautics and Space Administration, 1967.
[60] J.C. Amazigo, B. Budiansky, Asymptotic formulas for the buckling stresses of axially compressed cylinders with localized or random axisymmetric imperfections, J. Appl. Mech. 39 (1) (1972) 179–184.